

# Photonic superlattices for photonic crystal lasers

Koen Clays\*, Kasper Baert, Mark Van der Auweraer, Renaud Vallée

Department of Chemistry and Institute of Nanoscale Physics and Chemistry (INPAC), Katholieke Universiteit Leuven, Celestijnenlaan 200D, Leuven 3001, Belgium

## ABSTRACT

Colloidal photonic crystals, even with low refractive index contrast have a significant effect on the spontaneous emission of internal emitters. This is observed as a modification of the emitters' fluorescence spectrum and as a narrowing and shortening of the decay rate distribution. The decay rates are observed to be nonexponential. This modification was then put to use by fabricating a photonic superlattice, consisting of several photonic crystal slabs deposited on top of each other. Because of the two different photonic bandgaps and effective passband is created between the two and leads to enhancement of emission in this spectral region. These experiments indicate that the threshold for lasing can possibly be lowered by spectrally narrowing the emission of fluorophores infiltrated in suitably engineered self-assembled photonic crystal superlattices, and are therefore important towards the realization of efficient all-optical integrated circuits from functionalized photonic superlattices and heterostructures.

**Keywords:** Photonic crystals, photoluminescence, spectral narrowing, inhibited spontaneous emission, nonexponential decay, superlattices

## 1. INTRODUCTION

Periodic dielectric structures, known as photonic crystals (PCs), have been predicted to radically change the photonic local density of states (LDOS), which governs the interaction between the emitter and the electric field in the structure.<sup>1</sup> The achievement of a photonic band gap (PBG), *i.e.*, a range of frequencies for which the LDOS vanishes, is an active field of research. To engineer a three dimensional (3D) PBG material, the periodicity of the refractive index should be realized in 3D. Physical top-down approaches are less amenable to such PBG structures. Chemical self-assembly of colloidal particles, on the other hand, is particularly well suited toward close-packed 3D photonic crystals. The self-assembly results in the thermodynamically most stable face-centered cubic (fcc) crystal structure or in the (random) hexagonal closed packing (Rhcp) crystal structure, both with a packing of 74%. The size of the colloidal particles, together with the refractive index, determines the spectral position of the band gap. The combination of these dense crystal structures (fcc or Rhcp) with the low refractive index of most colloidal particles (latex and silica) results in an incomplete band gap (pseudogap or stop band).<sup>2</sup> For a complete band gap, *i.e.*, a forbidden spectral region for all incidence angles, either a more effective crystal structure (diamond structure),<sup>3,4</sup> less dense packing (inverted opals), or higher refractive index contrast (*e.g.*, titania or zirconia particles) is necessary.<sup>5,6</sup>

Because of the difficulties in sample fabrication, most of the experimental studies concerning the emission properties of atoms, molecules, and/or quantum dots in PCs have been achieved only in 3D PC's with pseudogaps (pseudo-PBG's). The first report of the inhibition of the spontaneous emission rate in a PC (Ref. 7) turned out to be due to non-PC effects.<sup>8</sup> Recently, wide lifetime distributions containing both enhanced and inhibited decay components were reported for dyes (NBIA) embedded in a polymer network filling the voids of an opal structure.<sup>9</sup> In this experiment, the dye molecules were spread homogeneously over the sample. However, if the dye molecules are homogeneously embedded in a spherical layer inside the silica spheres for a similar system,<sup>10</sup> only a single decay lifetime was found, slightly changed with respect to the reference sample. These contradictory results concerning the influence of the stop band on the radiative lifetime of the emitters have been extensively discussed.<sup>11-15</sup> More recently, depending on the emission frequency, lifetime fluctuations up to 30% have been reported<sup>16</sup> for CdSe quantum dots in inverse PCs. Furthermore, nonexponential decay profiles of quantum dots embedded in 3D fcc inverse opals have been experimentally observed. The profiles have been analyzed in terms of a continuous distribution of decay rates. Very interestingly, the widths of these distributions have been related to the variation of the LDOS at the various positions and orientations of the emitter in the unit cell.<sup>17,18,19</sup>

In this context, it is still unclear whether PCs with relatively low dielectric contrast (as it is the case for most opal structures) can have significant influence on the emission rate of internal emitters. Additionally, defects in the crystal structure can lead to changes in the observed fluorescence spectra, due to diffuse scattered light,<sup>20</sup> making a real quantitative analysis difficult. It is the purpose of this paper to provide such a detailed analysis, combining both macroscopic and microscopic experimental investigations of dyes embedded in silica opals. We show that the normalized emission spectra of the molecules have a shape varying with the lateral position of the investigated ensemble of emitters in the sample. Furthermore, the decay profiles of these ensembles of emitters show indeed a nonexponential behavior, with an extent that depends on the lattice constant of the grown PC, and are best described by a continuous distribution of decay rates.<sup>17,18,19</sup> These distributions of decay time vary slightly from position to position in the sample, indicating slight heterogeneities in the structures.

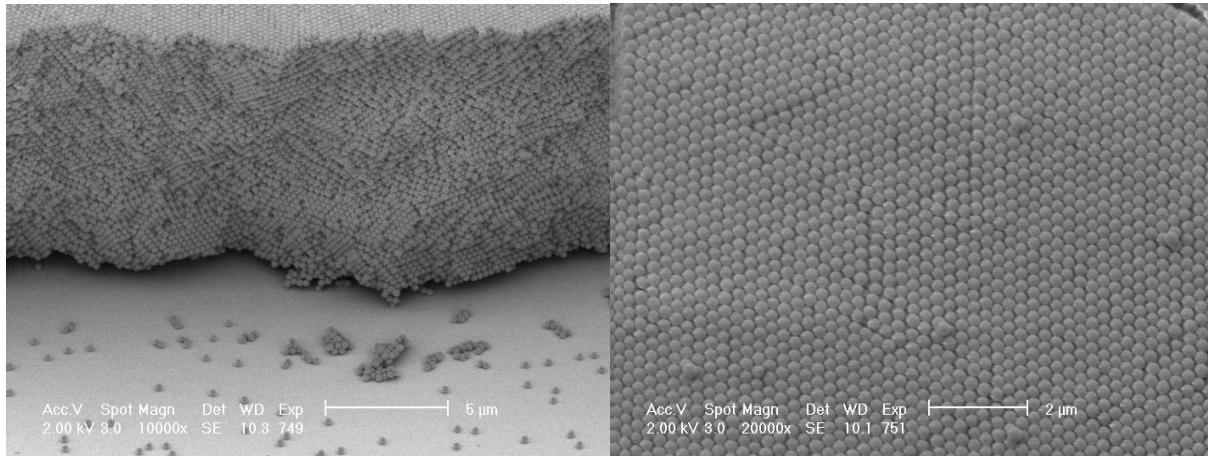


Fig. 1. Scanning electron microscope views of a PSB colloidal crystal obtained by convective self-assembly from a colloidal dispersion (size of the particles: 260 nm). Left: Transversal view. Right: Top view.

A further accomplishment in the design of PBG materials is the realization of a passband inside the bandgap,<sup>21</sup> to allow an emission narrowing of the inserted fluorophores and possibly lasing of the photonic crystal. By engineering lower-dimensional intentional defects in a photonic crystal, the bandgap can be designed to have allowed passband defect modes. While it is difficult to introduce such defects by physical top-down lithographic techniques, interfacial self-assembly techniques are naturally effective in introducing 2D defect layers in 3D colloidal crystals. By introducing a monolayer of particles of different size or different refractive index in a photonic crystal, it is possible to impart a passband in the stopband.<sup>22,23,24</sup>

While we have succeeded to insert a passband in a stopband by introducing a monolayer defect of silica particles of different size by using the Langmuir-Blodgett interfacial technique,<sup>22,23,24</sup> the partial nature of the passband that is realized in this way does not allow its observation in fluorescence emission. The engineered passband shows up as a narrow dip in a single, narrow stopband. The spectral position of this dip and stopband is dependent on the angle of incidence of the light. Therefore, for detection with omnidirectional emission, the narrow band is washed out. Therefore, we reverted to a different strategy that would impart a stronger (deeper and wider) allowed passband in a broad forbidden range of wavelengths, resulting from an engineered effective stopband. The stopband results from the linear addition of the individual stopbands from slabs of photonic crystals made from colloidal particles with different size. By proper choice of the relative particle sizes in such a photonic superlattice, the effective width of total stopband and passband within the stopband can be tuned.

## 2. EXPERIMENTS

### 2.1 Photonic crystal preparation

Monodisperse spherical silica particles with diameters of 171 nm for the reference sample, 260 nm for the photonic stop band (PSB) samples and 250 nm (A) and 260 nm (B) for the superlattice samples were produced by a strict control of the conditions for the well-known Stöber method.<sup>25</sup> After completion of the hydrolysis of the tetraethylorthosilicate, followed by the condensation to silica, the colloidal suspension is centrifuged and resuspended in ethanol by sonication four times. The convective self-assembly process makes use of the suspending power of ethanol for these silica particles, in combination with an appropriate vapor pressure for this solvent at 305 K.<sup>26</sup> The glass substrate and the vial containing the suspension are cleaned with piranha acid (2/3 sulphuric acid, 1/3 hydrogen peroxide as oxidant) prior to use. The substrate is placed vertically in the vial. Photonic AB and ABAB superlattices were made by successive deposition of photonic crystal slabs composed of colloidal particles of the two different sizes. The slabs were deposited out of an ethanolic suspension of approximately 0.3 %vol (sample 1, reference sample with photonic bandgap at 376 nm; sample 2, PSB sample with a photonic bandgap at 566 nm; sample 3, AB thin-slab photonic superlattice) or 0.6 %vol (sample 4, ABAB thick-slab photonic superlattice). The slab superlattice structure of the samples is schematically represented in Figs. 10a and 11a, for samples 3, and 4 respectively. The multiple-slab ABAB superlattices were prepared to investigate the effect of the emission being preferentially collected through one side of the crystal. It also allowed controlling the linear additivity of the individual bandgaps. Figure 1 shows transversal (left) and top (right) views of a PSB colloidal crystal obtained by using a scanning electron microscope (Philips XL30 ESEM FEG). The figure allows one to judge the good quality of the 10  $\mu\text{m}$  thick crystal constituted by 42 layers of colloidal particles.

After each deposition of a single slab, the resulting structure was dried at approximately 403 K to remove any residual solvent. The photonic superlattices exhibit dual photonic bandgaps resulting from the linear combination of the bandgaps of the individual stacks (A at 532 and B at 577 nm, respectively).<sup>27</sup>

It has been reported that the insertion of a defect layer of larger particle diameter in between two slabs made up of particles with smaller diameter results in increased disorder for a diameter ratio of 1.5.<sup>24</sup> The difference in particle size here is only 4 %, allowing for a (quasi) epitaxial growth of particles of both diameters upon each other. While the interface between each two slabs could be considered as a defect, the effectively observed passband is not a true defect mode. The passband simply results from the superposition of two spectrally shifted stopbands. In between the two stopbands, a net resulting allowed passband emerges.

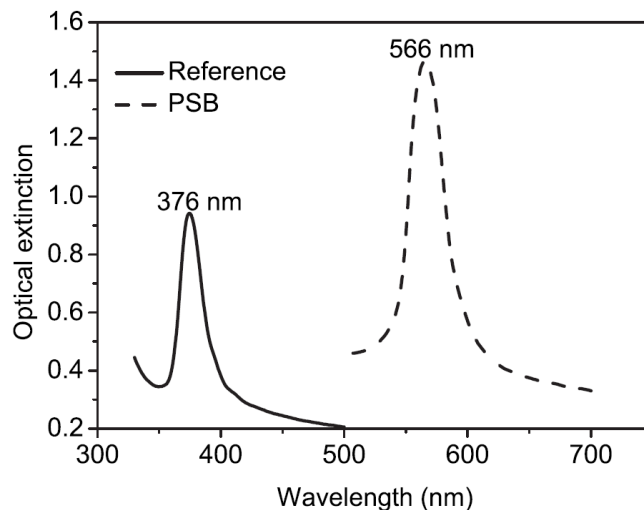


Fig. 2. Extinction spectra for photonic crystal samples 1 and 2: respectively reference (solid) and photonic stop band (PSB, dash). The reference sample has its stop band outside the emission spectral region, while the PSB sample has its stop band in the emission spectral region.

## 2.2 Optical extinction spectra

Optical extinction spectra were performed on large areas (millimeter sized) to ascertain the quality and spectral features of the samples using a Perkin-Elmer Lambda 900 UV-VIS-NIR spectrophotometer. The optical extinction spectra are shown in Figures 2-4.

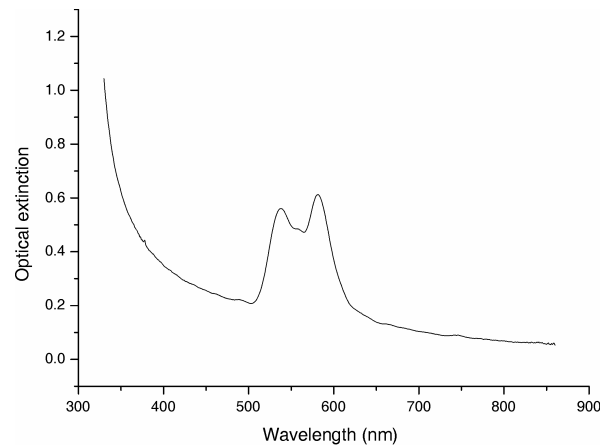


Fig. 3. Extinction spectrum of the photonic crystal sample 3: AB thin-slab superlattice photonic crystal with engineered forbidden stopband and allowed passband in stopband in emission spectral region.

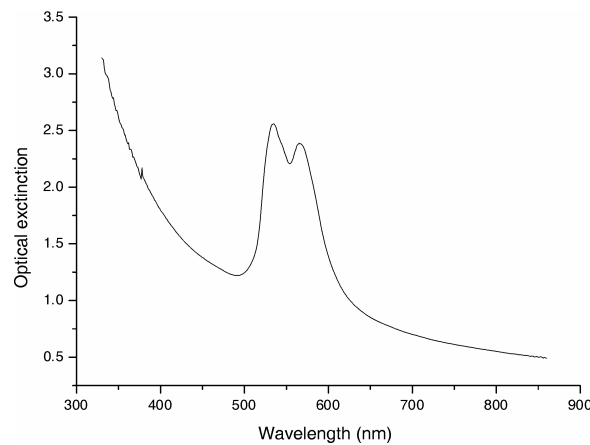


Fig. 4. Extinction spectrum of the photonic crystal sample 4: ABAB thick-slab superlattice photonic crystal with engineered forbidden stopband and allowed passband in stopband in emission spectral region.

The spectral properties of the passband stopband combination obtained by this approach are compared with those obtained from a true monolayer defect mode between two identical crystal stacks<sup>23</sup> in Table I. With our new multiple-slab approach, we have been able to engineer a wider stopband (twice as wide), with a more pronounced (twice as wide and 50% more amplitude) passband.

## 2.3 Fluorescence emission spectra

In order to investigate the effect of the stop band on the emission properties of fluorophores, disodium fluorescein molecules were postinfiltrated in the colloidal crystals. Reference samples were grown from smaller silica spheres in order to present a stop band out of the visible range spanning the emission of the fluorophores. This allowed us to compare their emission properties with those in the effectively active (PSB) sample with a photonic stop band in the visible range. The disodium fluorescein molecules have a fluorescence quantum yield  $\Phi=0.97$  in basic ethanol, an emission spectrum spanning a spectral range from 500 to 700 nm, *i.e.*, covering the spectral range of the stop band of the PSB samples (expected maximum at 565 nm) and a fluorescence lifetime of 4 ns. The infiltration was performed by placing the crystals in a  $1.1 \times 10^{-3}$  M solution of the fluorescein in methanol for 30 min.

Table I. Comparison of spectral properties for designed passband in stopband obtained by two different engineering approaches

Crystal type	Two stacks of different particle size, no monolayer	Monolayer defect of different particle size in between two stacks of identical particle size
Passband nature	Gap between two stopbands	Passband defect mode
Central position stopband (nm)	556	635
FWHM total stopband (FWHM, nm cm <sup>-1</sup> )	80 2600	50 1228
Position passband (nm)	532	632
FWHM passband (FWHM, nm cm <sup>-1</sup> )	19 612	10 260
Relative amplitude passband/stopband	0.25 25%	0.17 17%

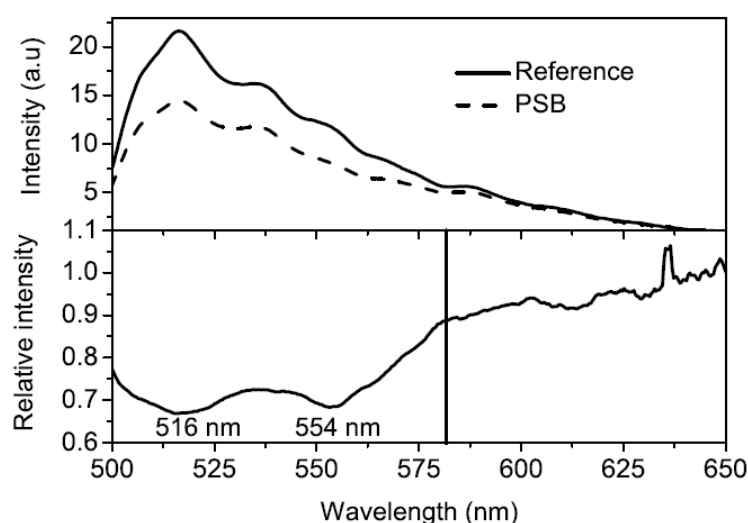


Fig. 5. Averaged emission spectra of 18 ensembles of molecules located at 18 different positions in the reference (solid) or PSB (dash) samples (top) and corresponding relative emission spectrum (bottom). The dip in the relative emission spectrum is blue shifted (12 nm) with respect to the position of the stop band of the PSB sample (Fig. 2). The second dip at 516 nm is located at the peak position of the fluorescein emission spectrum.

The fluorescence experiments were performed with an inverted confocal scanning optical microscope (Olympus IX70). The excitation light, *i.e.*, pulses of 1.2 ps at a repetition rate of 8 MHz (Spectra Physics, Tsunami, Pulse Picker, and Doubler) and a wavelength  $\lambda=488$  nm, was circularly polarized and the power set to 10 nW at the entrance port of the microscope. The emission light was collected through the same objective [Olympus 0.5 NA (numerical aperture), 25x] used to focus the excitation light on the sample, in an epifluorescence configuration. The spatial resolution of the confocal microscope is then about 300 nm transversally (x and y directions) and about 1  $\mu\text{m}$  longitudinally (z direction). In order to eliminate any residual excitation signal in the fluorescence emission, a suitable combination of filters was used, consisting of a bandpass (BP488, Chroma) placed in the excitation path, a dichroic (Olympus 495), a notch (Kaiser Optics, 488) that matches the bandpass, and a long pass (LP505, Chroma) in the emission path. The emission spectra were recorded, with an integration time of 10 s, by a liquid-nitrogen-cooled backilluminated charge-coupled device (CCD) camera (LN/CCD-512SB, Princeton Instruments) coupled to a 150 mm polychromator (SpectraPro 150, Acton Research Cooperation). Furthermore, an additional dichroic mirror (Olympus 570) was placed in the emission path in order to separate the emission originating from photons with a transition frequency in ( $\lambda < 570$  nm) and out [ $\lambda > 580$  nm, with an additional long pass filter (LP580, Chroma)] of the stop band of the PSB sample. The split signals were sent to two avalanche photodiodes (SPCM-AQ-14, EG & G Electro Optics) equipped with a time-correlated single photon counting card (Becker & Hickl GmbH, SPC 630) used in the first in first out (FIFO) mode to measure the time lags

between excitation and emission. A suitable window of 16.1 ns (time width of 63 ps per channel for the 256 channels available in the FIFO mode) was chosen to adequately build the decay profiles.

The samples were oriented so that the PC lattices have their [111] axis along the z direction of the microscope, *i.e.*, with the crystal top side oriented toward the objective lens of the microscope. Neither the excitation nor the emitted light passed through the glass substrate with this backward detection scheme. As mentioned in the literature already,<sup>28</sup> the main advantage of such a microscopic approach, as compared to macroscopic investigations, is its ability to probe the crystal structure locally. As the main intensity of the excitation laser beam is focused to a diffraction limited spot, only molecules within a small sample volume contribute to the detected fluorescence signal. Varying the focus position laterally provides direct information on the local quality of the crystal domains and/or distribution of molecules in the sample volume.

## 2.4 Spontaneous emission rates

Besides getting the emission spectra at different positions in the samples, our setup allows us to also determine fluorescence decays (single photon timing) by recording the histograms of the time lags between excitation photons and fluorescence photons. In order to distinguish between photons emitted at a transition frequency in (mainly  $\lambda < 570$  nm) and out ( $\lambda > 580$  nm) of the range of the dip of the PSB emission spectrum (Fig. 5), we determined the fluorescence decays collected for both wavelength ranges. Figure 6 shows the fluorescence decays of all photons emitted at a particular position of a reference (closed triangles) and PSB (open triangles) samples. Clearly, the decays exhibit a nonexponential behavior. The origin of such nonexponential behavior has been discussed recently in the literature in the case of quantum dots embedded in fcc inverse opals consisting of air spheres in a titania backbone.<sup>17,18,19</sup>

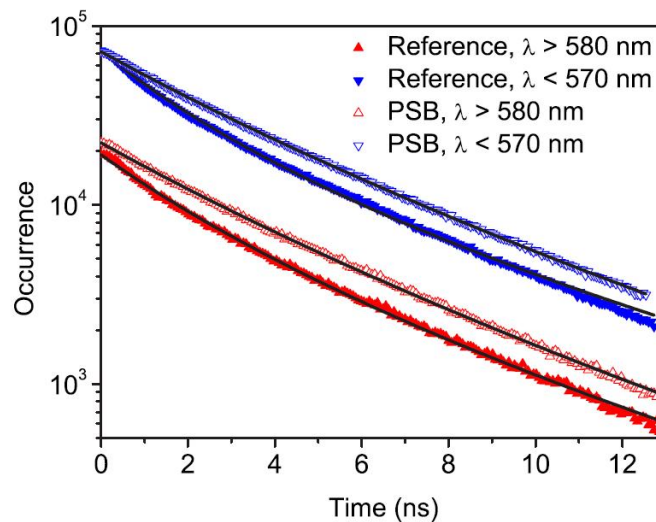


Fig. 6. Decay profiles of ensembles of emitters located either in a reference (closed triangles) or in a PSB (open triangles) sample. The time lags between excitation and emission have been recorded in two different channels: the photons emitted with  $\lambda < 570$  nm (in the stop band of the PSB sample, down triangles) and  $\lambda > 580$  nm (outside the stop band of the PSB channel, up triangles) have been collected separately. Note the strong nonexponential decays displayed in this semilogarithm plot.

Accordingly, we applied the framework developed in Refs. 17 and 18 to analyze our results. The procedure consists in modeling the curves with a continuous distribution of decay rates:

$$I(t) = I(0) \int_{\gamma=0}^{\infty} \phi(\gamma) \exp(-\gamma t) d\gamma, \quad (1)$$

where  $\phi(\gamma)$  is the log-normal distribution of decay rates with dimension of time:

$$\phi(\gamma) = A \exp\left(-\frac{\ln^2\left(\frac{\gamma}{\gamma_{mf}}\right)}{w^2}\right), \quad (2)$$

where  $\gamma_{mf}$  is the most frequent decay rate corresponding to the maximum of  $\phi(\gamma)$ ,  $w$  is a dimensionless width parameter that determines the distribution width at  $1/e$ ,

$$\Delta\gamma = 2\gamma_{mf} \sinh(w) \quad (3)$$

and  $A$  is a normalization constant such that  $\int_{\gamma=0}^{\infty} \phi(\gamma) d\gamma = 1$ . The important feature of the log-normal distribution is its positiveness, which excludes the occurrence of unphysical negative decay rates and a full description in terms of only two parameters  $\gamma_{mf}$  and  $\Delta\gamma$ .

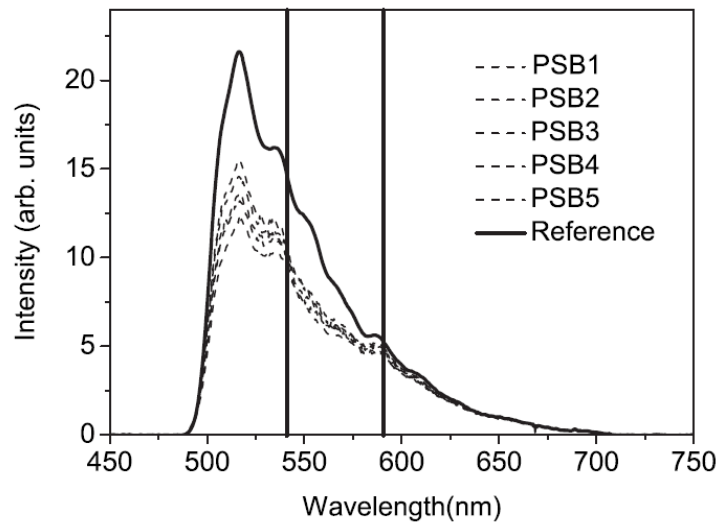


Fig. 7. Emission spectra of ensembles of molecules located at five different positions of a PSB sample (dash), among the 18 investigated. The solid line stands for the emission spectra averaged over ensembles of molecules located at 18 different positions of the reference sample.

### 3. RESULTS AND DISCUSSION

We used microscopic techniques to study the emission of fluorescein molecules in our photonic structures (reference and PSB samples). The recorded emission spectra are highly sensitive to the depth and lateral position of the focus (focal volume investigated) in the sample. As noticed in the literature already,<sup>28</sup> the dip in the emission intensity, usually related to the PSB, increased as the focus penetrated into the sample, according to the growing number of lattice planes between focus and detector. Furthermore, by moving the focus laterally while keeping it at a constant depth, the dip in the emission intensity was also affected, varying significantly from position to position in the sample. Fig. 7 shows the PSB emission spectra (dash) taken at 5 (among the 18 investigated) different positions within 2 distinct PSB samples. Also shown is the reference emission spectrum (solid) obtained by averaging 18 spectra corresponding to 18 positions taken randomly within 2 reference samples. All spectra are normalized to 1 at the wavelength  $\lambda = 650$  nm, *i.e.* outside (long wavelength range) the stop band exhibited by these structures (Fig. 7), in order to fairly compare them. The emission spectra of fluorescein in PSB clearly exhibit a qualitative change (of convexity) of the shape in the range 540 – 590 nm (where the stop band is active) with respect to the reference emission spectrum. This change manifests as a dip, with a depth depending on the lateral position in the PSB sample where the recording of the emission spectrum took

place. Interestingly, a significant dip is also observable at lower wavelength, namely at the peak position of the emission spectrum ( $\lambda = 516$  nm), where the effect of the stop band is normally vanished.

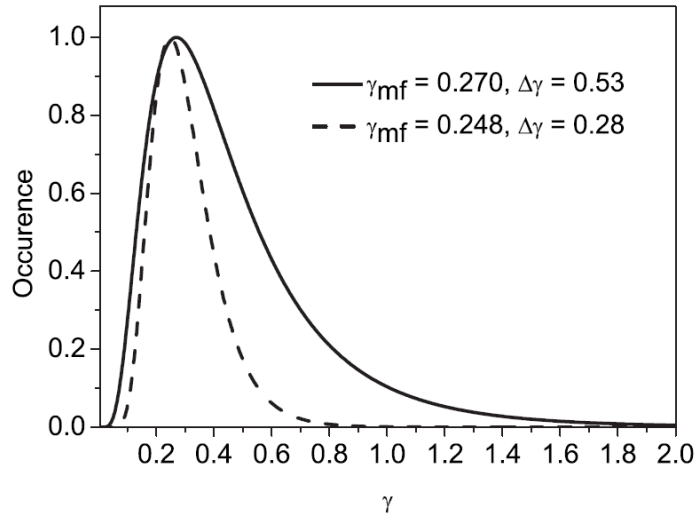


Fig. 8. Continuous distributions of decay rates obtained in the fitting of the nonexponential decay profiles shown in Fig. 5. The two curves correspond to the decay profiles of an ensemble of molecules in the reference (solid) and PSB (dash) samples in the blue zone of the spectra ( $\lambda > 570$  nm).

In order to get a quantitative estimation of these dips, we calculated the averaged PSB emission spectrum (average of 18 spectra corresponding to 18 positions taken randomly within the 2 PSB samples investigated), normalized it to 1 at  $\lambda = 650$  nm and divided it by the averaged and normalized reference emission spectrum. Fig. 5 shows the results of these manipulations with the reference (solid) and PSB (dash) emission spectra on the top and the divided spectrum on the bottom of the figure. The two above mentioned dips are located at  $\lambda = 516$  nm, *i.e.* precisely at the peak maximum of the fluorescein emission spectrum and  $\lambda = 554$  nm. The latter dip is slightly blue shifted with respect to the peak maximum of the stop band of the PSB sample ( $\lambda = 566$  nm, Fig. 1), as already noticed previously.<sup>29</sup>

From the single photon timing data we observed the nonexponential character of the fluorescence decays exhibited by the fluorescein embedded in our PC samples. Similar phenomena have been discussed recently in references<sup>17,18,19</sup>. These authors attribute this complex behavior to one or more of the following four reasons: (i) As the emitters are distributed at different positions and orientations in the unit cell of a PC, they experience different local density of states (LDOSs); (ii) Single emitters may reveal a non exponential decay due to van Hove singularities in the LDOS;<sup>30</sup> (iii) Non exponential decays may appear if the emitters have more internal levels than the usually considered two level systems; (iv) Temporal fluctuations of the emitters environment on time-scales larger than the fluorescence lifetime can lead to apparent nonexponential decays.

At first glance, we may exclude reasons (ii) to (iv) to affect our results. Indeed, van Hove singularities in the LDOS can only be observed with single molecule experiments, which is not the case here. Furthermore, the fluorescein molecules used in this study have a quantum yield of  $\Phi = 0.97$ , which rules out practically the contribution of any non radiative decay channel, and have a single exponential decay with a lifetime of 4 ns in ethanol. This suggests that even relative large intermolecular fluctuations in the rate of the non-radiative decay will only marginally influence the fluorescence decays. We are thus left with reason (i) as the possible cause of the non exponential decays observed in Fig. 6, *i.e.* the curves result from a distribution of radiative decay rates caused by a spatial and orientational variation of the LDOS.

Fig. 6 shows the excellent fits performed on the experimental decay curves, by use of the model discussed earlier. It is important to note here that neither a double exponential nor a stretched (KWW) exponential form was able to fit appropriately these curves. Fig. 8 shows the resulting decay rate distributions in the case of the two curves measured in the wavelength range  $\lambda < 570$  nm, *i.e.* in the spectral range where the PSB is active. Clearly, for the examples chosen, the distribution of decay rates measured at one position in the reference sample (solid) is much broader than the one in the PSB sample (dash). Also, the most frequent rates  $\gamma_{mf}$  slightly differ between the two samples. In order to investigate if such differences reflect the fact that we have a stop band (PSB sample) or not (reference sample) in the spectral zone of

interest or merely result from the heterogeneity of the samples, as already observed in the emission spectra (Fig. 7), we determined the decay-rate distributions at 18 positions both in the reference and PSB samples and for both spectral regions ( $\lambda < 570$  nm,  $\lambda > 580$  nm). Fig. 9 (left) shows the most frequent decay rates  $\gamma_{mf}$  (top) and widths  $\Delta\gamma$  (bottom) of these decay-rate distributions of an ensemble of molecules as a function of position in the reference (close triangles) and PSB (open triangles) and in the blue  $\lambda < 570$  nm (down triangles) and red  $\lambda > 580$  nm (up triangles) spectral ranges.

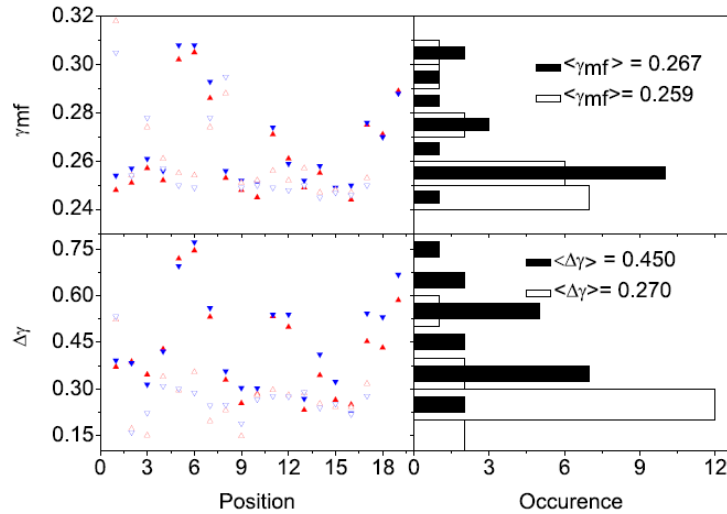


Fig. 9. Left: Most frequent decay rates  $\gamma_{mf}$  and widths  $\Delta\gamma$  of the continuous distributions of decay rates  $\phi(\gamma)$  for 18 ensembles of molecules measured at 18 different positions in the reference (close triangles) or PSB (open triangles) samples. The triangles down correspond to the mission at  $\lambda < 570$  nm (in the stop band of the PSB sample) and the triangles up correspond to the emission at  $\lambda > 580$  nm (outside the stop band of the PSB channel) of these ensembles of emitters. Right: Corresponding distributions of these two parameters in the blue zone of the spectra ( $\lambda < 570$  nm).

Fig. 9 exhibits several interesting features: (i) For both types of samples (reference and PSB) and both spectral ranges (blue and red), the distribution of the widths  $\Delta\gamma$  among various positions of the sample is much broader than that of the most frequent rates  $\gamma_{mf}$ ; (ii) For PSB (reference) samples, the widths of the decay-rate distributions are (twice) as large as the most frequent rates; (iii) In most cases (all minus 1), the  $\gamma_{mf}$  corresponding to ensembles of molecules located in the reference sample in the red spectral zone (close up triangles) are smaller than or equal to the corresponding ones in the blue spectral zone (close down triangles); (iv) Conversely, most (all minus three)  $\gamma_{mf}$  corresponding to ensembles of molecules located in the PSB sample in the red spectral zone (open up triangles) are larger than the corresponding ones in the blue spectral zone (open down triangles). These observations are further exemplified on the right side of Fig.6, which shows the distributions of the  $\gamma_{mf}$  and  $\Delta\gamma$  of ensembles of molecules located in the reference (solid) and PSB (dash) samples in the blue spectral range, *i.e.* for  $\lambda < 570$  nm where the PSB is active.

These observations exemplify the power of the approach, in giving detailed physical information on decay rates. They point (i) to the heterogeneity of the samples on the local scale and (ii) to the fact that the reference samples seem more heterogeneous than the PSB samples. Furthermore, the dependence of the rate  $\gamma \sim \omega^3$  on the third power of the transition frequency  $\omega$  for emitters embedded in an effective homogeneous medium (EHM, the reference sample has its stop band out of the emission range of the emitter and so acts as a EHM in the considered range) explains the observation (iii) that the largest  $\gamma_{mf}$  are observed for the largest transition frequencies collected. Finally, we conjecture that the converse observation (iv) of the smallest  $\gamma_{mf}$  observed for the largest transition frequencies collected in the case of emitters in the PSB sample results from the stop band active in the zone  $\lambda < 570$  nm (Fig. 1), which inhibits the emission of the molecules having their transition frequency in this range (LDOS effect).

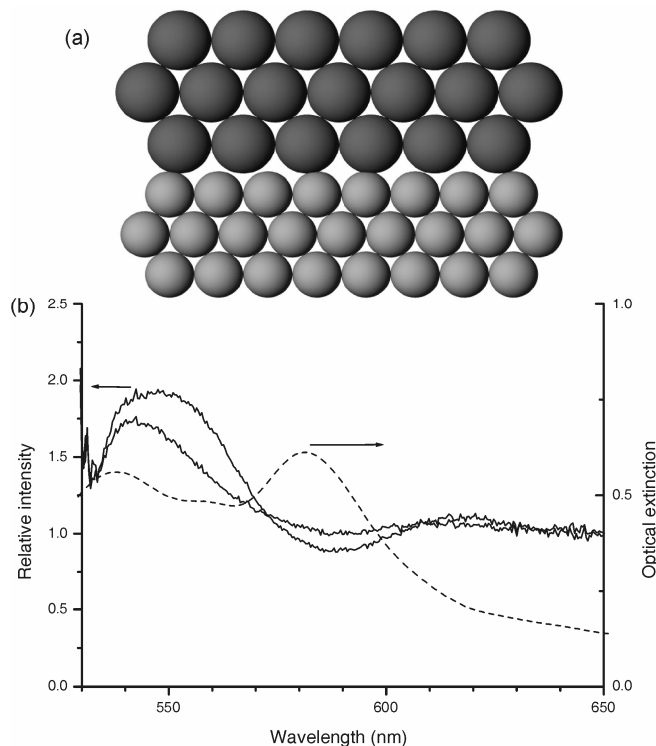


Fig. 10. (a) Schematic representation of thin-slab AB photonic superlattice sample 3. (b) Relative emission spectrum for thin-slab AB photonic superlattice sample 3 (solid lines, different positions in sample, left axis), compared with extinction spectrum (at  $0^\circ$  incidence angle, dotted line, right axis).

To study the effect of an allowed passband in an engineered broad stopband, two different photonic crystal samples with AB superlattice were studied (with long pass filter at 520 nm). For sample 3, an AB thin-slab superlattice with passband located at 550 nm in a broad stopband covering the range from 500 to 600 nm and showing a very weak miniband<sup>31,32</sup> (see extinction spectrum in Fig. 3), we very clearly observe a suppression of the emission in the right stopband region of 570 to 600 nm, with a maximum suppression (to the right) at approximately the extinction maximum (to the right). At the same time, an enhancement of the emission intensity in the allowed passband region around 550 nm is also observed. The dotted line in Fig. 10 represents the extinction spectrum. The two solid lines represent relative emission spectra at two different confocal positions in the sample, both close to the glass substrate. Both emission spectra clearly show the suppression and the enhancement of the emission at the appropriate spectral regions (stopband and passband, respectively). Please note that these emission spectra were taken with a long pass filter at 520 nm, precluding the observation of the full emission spectrum (to the left of the passband) of the fluorophore for samples 3 and 4. However, the onset of the emission suppression to the left of the passband at below 540 nm is clearly discernible for all three samples, with the very sharp cut-off dichroic having a 90% transmission already at 525 nm and a 95% transmission from 530 nm onwards.

Since sample 3 did exhibit miniband features in the passband, which could weaken the effect or complicate the analysis, we also made sample 4, a thick-slab ABAB superlattice. This 4-layer sample also minimizes the spectral effect of the emission being collected preferentially through one side of the crystal. As expected, the main spectral features (both the combined photonic band gap features and the Rayleigh scattering background) are enhanced in amplitude, while the miniband has disappeared indeed in the extinction spectrum (Fig. 4). Correspondingly, the effect of this more pronounced extinction spectrum on the emission is also enhanced with respect to sample 3. Figure 11 very clearly shows the fluorescence suppression in the region of 570 to 600 nm, and the fluorescence enhancement around 550 nm.

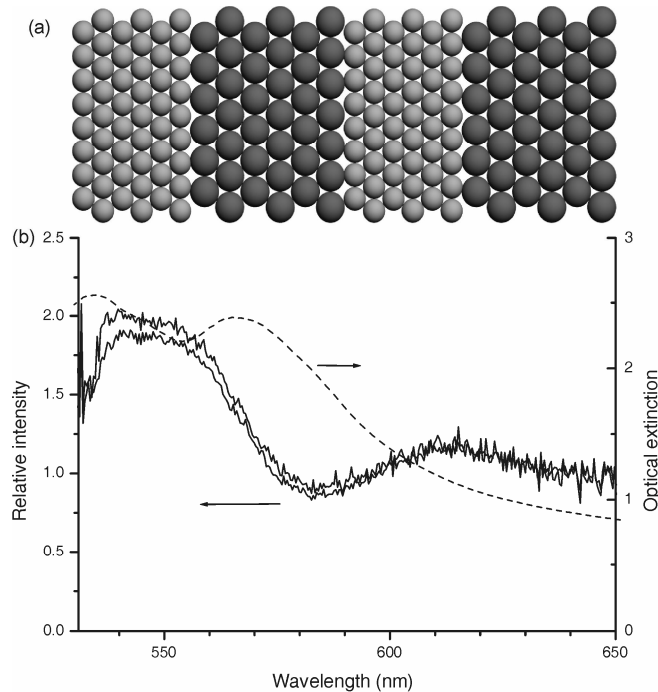


Fig. 11. (a) Schematic representation of thick-slab ABAB photonic superlattice sample 4. (b) Relative emission spectrum for thick-slab photonic superlattice sample 4 (solid lines, different positions in sample, left axis), compared with extinction spectrum (at  $0^\circ$  incidence angle, dotted line, right axis)

The extinction spectra of the samples clearly show the additivity of the bandgaps that are caused by the different slabs in the complete photonic crystal. Also, comparison of the emission spectra from both the thin-slab samples AB and ABAB show that there is no significant effect of the asymmetry of the sample.

#### 4. CONCLUSIONS

We have shown here that PCs with relatively low dielectric contrast can have significant influence on the emission rate of internal emitters. Decay profiles of ensembles of emitters measured at different positions in the PCs have exhibited a non exponential behavior (Fig. 6). These non exponential profiles have been best fitted by continuous distributions of decay rates (Fig. 8) and have been attributed, as previously done for ensembles of quantum dots in inverse opals,<sup>17,18</sup> to spatial and orientational variations of the LDOS in the unit cells. The two parameters of the continuous distributions of decay rates, the most frequent decay rate  $\gamma_{mf}$  and the width  $\Delta\gamma$  of the distribution, have been shown to slightly vary from position to position in each sample, and also, in a larger extent, when measured either in the reference or PSB samples. These slight variations as a function of position in the same sample can only be attributed to some local imperfections in the structure or difference in the concentration of fluorophores at these positions. The latter effects are supposed to also give rise to the various spectra observed as a function of position in a given sample (Fig. 7).

We have successfully implemented a strategy to produce, by convective self-assembly, a pre-designed broad effective stopband with a well-pronounced allowed passband in this forbidden photonic stopband. We have experimentally shown spectral narrowing by such a well-designed passband in the stopband of a self-assembled colloidal photonic superlattice. The importance of this result can be appreciated by considering the wide spectral range of the suppression (the width of the effective stopband, from 500 to 600 nm) covering the spectral breath of fluorophore emission, in combination with the narrow range of the enhanced emission (FWHM of relative emission spectra of Figs. 10b and 11b approximately 30 nm) that can be sufficient to suppress all but one lasing mode in small optically integrated devices. Spectral narrowing and spectral collapse into a single mode is often considered as the first indication of lasing. Therefore, we have shown that properly engineered self-assembled colloidal photonic superlattices could become good candidates for low-threshold and/or single mode photonic crystal lasers.

Towards the development of self-assembled colloidal photonic crystal lasers, the realization of feedback structures at the design wavelength asks for Bragg reflectors (narrow stopbands) at both ends of the engineered photonic crystals at the lasing wavelength, in combination with the allowed passband at the same design wavelength, in a broad stopband extending over the emission spectrum of the fluorophore, realized in a double stack that constitutes the central part of the lasing crystal. To limit the designed functionality to the envisioned photonic crystal part (feedback only in two extreme crystal stacks, narrowed emission in central double stack), the fluorophores need to be nanostructured in the latter part, instead of post-infiltrated in the total crystal structure (including extreme feedback stacks). This can be realized by functionalization by covalent chemical bonds of silica particles with fluorophores with the appropriate chemical functional group (*e.g.*, isocyanate).<sup>33</sup>

## ACKNOWLEDGMENTS

P. Dedecker and M. Sliwa are acknowledged for help in aligning the setup. The authors thank the Research Fund of the KULeuven for financial support through GOA2006/2 and GOA2006/3, ZWAP 4/07 and the Belgium Science Policy through IAP 5/03. The Fonds voor Wetenschappelijk Onderzoek Vlaanderen is thanked for Grants No. G.0421.03 and No. G.0458.06.

## REFERENCES

1. E. Yablonovitch, Phys. Rev. Lett. **58**, 2059 (1987).
2. K. Wostyn, Y. Zhao, B. Yee, G. de Schaetzen, L. Hellemans, K. Clays, and A. Persoons, J. Chem. Phys. **118**, 10752 (2003).
3. K. M. Ho, C. T. Chan, and C. M. Soukoulis, Phys. Rev. Lett. **65**, 3152 (1990).
4. K. Busch and S. John, Phys. Rev. E **58**, 3896 (1998).
5. M. M. Sigalas, C. M. Soukoulis, R. Biswas, and K. M. Ho, Phys. Rev. B **56**, 959 (1997).
6. K. Busch and S. John, Phys. Rev. Lett. **83**, 967 (1999).
7. J. Martorell and N. M. Lawandy, Phys. Rev. Lett. **65**, 1877 (1990).
8. B.Y. Tong et al., J. Opt. Soc. Am. B **10**, 356 (1993).
9. E. P. Petrov et al., Phys. Rev. Lett. **81**, 77 (1998).
10. M. Megens et al., Phys. Rev. A **59**, 4727 (1999).
11. M. Megens et al., Phys. Rev. Lett. **83**, 5401 (1999).
12. E. P. Petrov et al., Phys. Rev. Lett. **83**, 5402 (1999).
13. Z. Y. Li and Z. Q. Zhang, Phys. Rev. B **63**, 125106 (2001).
14. X. H. Wang, R. Wang, B. Y. Gu, and G. Z. Yang, Phys. Rev. Lett. **88**, 093902 (2002).
15. S. Y. Zhu, G. X. Li, Y. P. Yang, and F. L. Li, Europhys. Lett. **62**, 210 (2003).
16. P. Lodahl, A. F. van Driel, I. S. Nikolaev, A. Irman, K. Overaa, D. Vanmaekelbergh, and W. L. Vos, Nature **430**, 654 (2004).
17. A. F. van Driel, I. S. Nikolaev, P. Vergeer, P. Lodahl, D. Vanmaekelbergh, and W. L. Vos, Phys. Rev. B **75**, 035329 (2007).
18. I. S. Nikolaev, P. Lodahl, A. F. van Driel, A. F. Koenderink, and W. L. Vos, Phys. Rev. B **75**, 115302 (2007).
19. R. A. L. Vallee, K. Baert, B. Kolaric, M. Van der Auweraer, and K. Clays, Phys. Rev. B **76**, 045113 (2007).
20. A. F. Koenderink and W. L. Vos, Phys. Rev. Lett. **91**, 213902 (2003).
21. E. Yablonovitch, T. J. Gmitter, R. D. Meade, A. M. Rappe, K. D. Brommer, J. D. Joannopoulos, Phys. Rev. Lett. **67**, 3380 (1991).
22. Y. Zhao, K. Wostyn, G. de Schaetzen, K. Clays, L. Hellemans, A. Persoons, M. Szekeres, R. A. Schoonheydt, Appl. Phys. Lett. **82**, 3764 (2003).
23. K. Wostyn, Y. Zhao, G. de Schaetzen, L. Hellemans, N. Matsuda, K. Clays, and A. Persoons, Langmuir **19**, 4465 (2003).
24. P. Massé, S. Reculosa, K. Clays, S. Ravaine, Chem. Phys. Lett. **422**, 251 (2006).
25. W. Stöber, A. Fink, and E. Bohn, J. Colloid Interface Sci. **26**, 62 (1968).
26. P. Jiang, J. F. Bertone, K. S. Hwang, and V. L. Colvin, Chem. Mater. **11**, 2132 (1999).
27. S. Reculosa, P. Massé, S. Ravaine, J. Coll. Interf. Sci. **279**, 471 (2004).
28. M. Barth, A. Gruber, F. Cichos, Phys. Rev. B **72**, 085129 (2005).
29. K. Baert, K. Song, R.A.L. Vallée, M. Van der Auweraer, K. Clays, J. Appl. Phys. **100**, 123112 (2006).
30. N. Vats, S. John, and K. Busch, Phys. Rev. A **65**, 043808 (2002).
31. R. Rengarajan, P. Jiang, D. C. Larrabee, C. L. Colvin, D. M. Mittleman, Phys. Rev. B., **64**, 205103 (2001).
32. P. Jiang, G. N. Ostojic, R. Narat, D. M. Mittleman, V. L. Colvin, Adv. Mat., **13**, 389 (2001).
33. K. Song, R. Vallée, M. Van der Auweraer, K. Clays, Chem. Phys. Lett. **421**, 1 (2006).